Organosilicon phantom for photoacoustic imaging

Cinzia Avigo
Nicole Di Lascio
Paolo Armanetti
Claudia Kusmic
Lucia Cavigli
Fulvio Ratto
Sandro Meucci
Cecilia Masciullo
Marco Cecchini
Roberto Pini
Francesco Faita
Luca Menichetti

Organosilicon phantom for photoacoustic imaging

Cinzia Avigo,[a,†] Nicole Di Lascio,[a,b,†] Paolo Armanetti,[c] Claudia Kusmic,[a] Lucia Cavigli,[d] Fulvio Ratto,[d] Sandro Meucci,[e,f] Cecilia Masciullo,[e] Marco Cecchini,[e] Roberto Pini,[d] Francesco Faita,[a] and Luca Menichetti[a,g,*]

[a]Istituto di Fisiologia Clinica, CNR, Via Giuseppe Moruzzi 1, Pisa 56124, Italy
[b]Scuola Superiore Sant'Anna, Piazza Martiri della Libertà 33, Pisa 56127, Italy
[c]Università di Pisa, Dipartimento di Fisica, Largo Bruno Pontecorvo 3, Pisa 56127, Italy
[d]Istituto di Fisica Applicata "Nello Carrara," CNR, Via Madonna del Piano 10, Sesto Fiorentino (FI) 50019, Italy
[e]NEST, Istituto Nanoscienze, CNR and Scuola Normale Superiore, Piazza San Silvestro 12, Pisa 56127, Italy
[f]Center of Nanotechnology Innovation @NEST, Istituto Italiano di Tecnologia, Piazza San Silvestro 12, Pisa 56127, Italy
[g]Fondazione CNR/Regione Toscana G. Monasterio, Via Giuseppe Moruzzi 1, Pisa 56124, Italy

Abstract. Photoacoustic imaging is an emerging technique. Although commercially available photoacoustic imaging systems currently exist, the technology is still in its infancy. Therefore, the design of stable phantoms is essential to achieve semiquantitative evaluation of the performance of a photoacoustic system and can help optimize the properties of contrast agents. We designed and developed a polydimethylsiloxane (PDMS) phantom with exceptionally fine geometry; the phantom was tested using photoacoustic experiments loaded with the standard indocyanine green dye and compared to an agar phantom pattern through polyethylene glycol-gold nanorods. The linearity of the photoacoustic signal with the nanoparticle number was assessed. The signal-to-noise ratio and contrast were employed as image quality parameters, and enhancements of up to 50 and up to 300%, respectively, were measured with the PDMS phantom with respect to the agar one. A tissue-mimicking (TM)-PDMS was prepared by adding TiO_2 and India ink; photoacoustic tests were performed in order to compare the signal generated by the TM-PDMS and the biological tissue. The PDMS phantom can become a particularly promising tool in the field of photoacoustics for the evaluation of the performance of a PA system and as a model of the structure of vascularized soft tissues. © *2015 Society of Photo-Optical Instrumentation Engineers (SPIE)* [DOI: 10.1117/1.JBO.20.4.046008]

1 Introduction

Photoacoustic (PA) imaging is an emerging technique that combines the high contrast and spectroscopic specificity of pure optical methods with the spatial resolution of ultrasound (US) imaging.[1,2] In PA imaging, US waves are generated by irradiating tissue with an optical excitation provided by a nanosecond pulsed laser. The absorption of light by endogenous chromophores, such as hemoglobin and melanin, or exogenous agents, such as organic dyes or plasmonic nanoparticles, produces a local increase in temperature.[1,2] This generates a consequent thermoelastic expansion resulting in broadband acoustic waves that can be detected using US receivers.

The use of contrast agents can enhance the sensitivity and the spectroscopic specificity of a PA signal and extend the range of applications of PA imaging to include the detection of specific molecular targets or selected tissues. A good contrast agent should exhibit stability, biocompatibility, specificity for a biological target of interest, and a large optical absorption cross-section at the wavelengths used for excitation.[3,4] Gold nanoparticles of various shapes demonstrated promising properties for biomedical applications:[5] in particular, gold nanorods (GNRs) have remarkable optical properties related to their surface plasmon resonance, which results in a strong optical absorption (one thousand times stronger than an equivalent

volume of an organic dye) and scattering at visible and near-infrared wavelengths.[6] Recent studies showed that GNRs exhibit minimal toxicity and are suitable for conjugation with ligands to gain molecular specificity.[7] For these reasons, GNRs have been used during the last years to enhance a PA signal, for example, in inflammatory cells, targeted cancer tissue, and sentinel lymph nodes.[5,8–14] In this work, we used GNRs with a peak absorption wavelength at 840 nm, prepared in our laboratories,[15] as a reference compound together with a conventional dye, i.e., indocyanine green (ICG).

Currently, PA imaging systems are commercially available; however, there is a lack of reference protocols and phantoms with fine geometry specially designed for semiquantitative evaluation of the performance of a PA system and for the assessment of the contrast enhancement provided by novel materials under different conditions of excitation wavelength, duration of irradiation, surrounding medium, dilution, and spatial distribution.

The aim of this work was to design and develop a polydimethylsiloxane (PDMS) device composed of micrometric channels for a semiquantitative evaluation of the performance of a PA imaging system using selected dyes (ICG) and/or nano-sized contrast agents (i.e., GNRs). A custom-made agar phantom was employed as the reference phantom. These two systems were filled with polyethylene glycol (PEG)-GNRs; the efficiency and stability of PA conversion under pulsed irradiation were

---

*Address all correspondence to: Luca Menichetti, E-mail: luca.menichetti@ifc.cnr.it

†Authors equally contributed to the manuscript.

studied and compared by using the commercial PA and micro-US imaging system Vevo LAZR (VisualSonics Inc., Toronto).

2 Materials and Methods

2.1 Phantom Description

Materials with suitable properties for use in both optical and US phantoms have been widely studied.[16–18] It was shown that hydrogels such as polyvinyl alcohol gel, polyacrylamide gel, gelatin with different additives, and agar can be effectively used for phantom design;[16] because they are mainly composed of water, they show low acoustic attenuation and impedance and speed of sound similar to those in biological tissue, as reported in Table 1.[19,20] Furthermore, the combined use of agents such as Indian ink or graphite powder providing optical absorption and titanium oxide or intralipids providing scattering, allows the realization of tissue-mimicking (TM) phantoms. However, hydrogels may suffer from dehydration and bacterial growth and are highly susceptible to physical damage.[16] In addition, water-soluble materials, such as dyes, diffuse in these gels; therefore, they require encapsulation in, for example, polyethylene tubes, creating an acoustic boundary. Moreover, preparing hydrogels containing microchannel structures is a great challenge.[21,22]

PDMS differs from hydrogels in that it is a soft, elastomeric material that belongs to the category of silicones. This material can be molded by standard soft lithography, it is stable for months and even years,[16] and it is durable against rough

handling, in contrast to hydrogels. Furthermore, like hydrogels, PDMS is nontoxic during preparation and application.[16] The PDMS thermoelastic expansion was exploited to produce high-frequency, broadband US;[25] moreover, PDMS was used for the preparation of tissue-simulating phantoms with tunable optical properties.[26,27] The optical and the acoustic properties of PDMS make it suitable for PA imaging since it is optically transparent and has a refractive index of ~1.43 in the near-infrared domain[26] (in the range of the refractive index of tissues), and its acoustic impedance is comparable to those of soft tissues (Table 1). The speed of sound of PDMS is ~12% lower than that in water and soft tissue, thus introducing a measurable but not significant artifact in the image reconstruction and superimposition of PA and US images. Furthermore, by adding some substances such as titanium dioxide and black ink to the PDMS, the absorption and reduced scattering coefficients can be tuned in order to be similar to those of biological tissues without compromising the phantom stability and stability against rough handling.[18,26]

Three types of phantoms were employed for PA experiments: the PDMS phantom (P1), the TM-PDMS phantom, and the agar-based (2%) phantom (P2), which was used as the control system.

P1 is a custom PDMS microfluidic device [Fig. 1(a)] composed of six parallel channels with sizes varying from 50 to 500 μm (in particular, 50, 100, 200, 300, 400, and 500 μm) and a thickness of 50 μm. The device was prepared by standard soft lithography. PDMS (Sylgard 184) was prepared by mixing the prepolymer and the curing agent at a ratio of 10∶1, pouring it into a custom-made microstructured mold, degassing to remove air bubbles, and baking at 80°C for 1 h. The replica was cut with a scalpel and removed from the master mold, and fluidic accesses to the microchannels were set up using a 0.75 mm Harris Uni-Core puncher. Subsequently, the floor of the channels was created by sealing the device to a glass coverslip. This process was done by activating the two surfaces using oxygen plasma (25 s, 1.4e-1 mbar, 10 W for the PDMS and 60 s, 1.4e-1 mbar, 100 W for the glass) and bringing them in conformal contact immediately after the treatment. A covalent bonding was formed in ~1 h, preventing leakages of liquid during liquid actuation. The PDMS phantom with microfluidic patterns could be cleaned with water and some acidic or organic solvents, but due to the micrometric channels, we cannot exclude a residual contamination, particularly when using nano-sized materials,

Table 1 Acoustic parameters of some tissues and water compared with agar and polydimethylsiloxane (PDMS).

Material	Impedance (KRayl)	Sound speed (m/s)	Density (g/cm^3)
Adipose tissue[23]	138	1450	0.95
Skeletal muscle[23]	166	1580	1.06
Water[23]	148	1482	0.99
PDMS[24]	150	1300	1.50
Agar[16]	157	1500	1.04
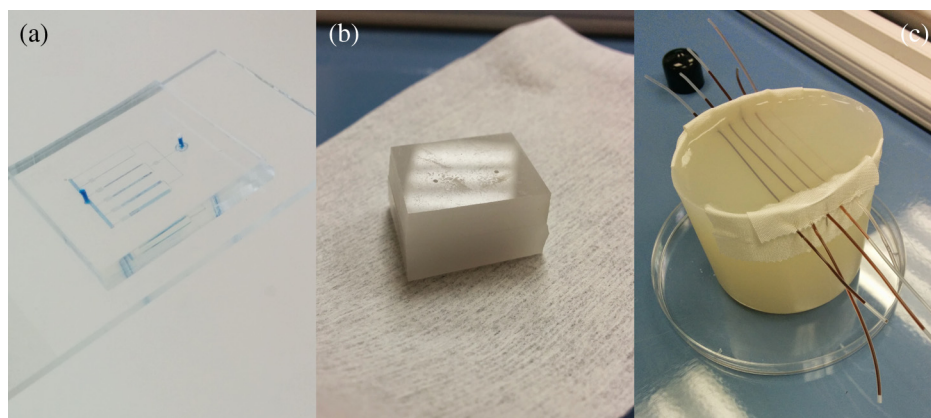
Fig. 1 (a) Polydimethylsiloxane (PDMS) phantom, (b) tissue-mimicking (TM)-PDMS phantom, and (c) agar phantom with five polyethylene tubes.

such as GNRs. The preparation of about five to six PDMS phantoms requires ~2 to 3 h.

The TM-PDMS phantom was realized by adding TiO$_2$ (0.73 mg/mL) to the curing agent and India ink (0.25 mg/mL) to the silicone [Fig. 1(b)].

P2 was used as the control system. The agar solution was poured into a custom-made cylindrical mold with up to five polyethylene tubes inserted and cooled down to room temperature until it solidified. The tubes (PE 50, micro medical tubing, 0.58 mm I.D. X 0.99 mm O.D.) were at a distance of 5 mm from each other and at a depth of 5 mm [Fig. 1(c)]. P2 was stored underwater at room temperature and was stable for several weeks.

All P1, TM-P1, and P2 were stable over the duration of testing (approximately one month). The background signal produced by P1 and P2 was checked by filling them with water.

2.2 Indocyanine Green

ICG-Pulsion (Pulsion, Munich, Germany) was used as the standard dye. The ICG powder was dissolved in a balanced salt solution at a concentration of 1 mM. The solution was protected from light and used a few hours after the preparation.

2.3 Gold Nanorods

Chemicals were purchased from Sigma Aldrich and were used as received. GNRs were prepared by the autocatalytic reduction of chloroauric acid by ascorbic acid in the presence of cetrimonium bromide, silver nitrate, and gold nuclei, as described in detail in Ref. 15. The nanoparticles obtained from the autocatalytic reduction were then grafted with PEG in a 100 mM acetate buffer at pH 5.0 containing 50 μM alpha mercapto omega methoxy PEG strands (MW ~5000 g mol^{-1}) and transferred into ultrapure water at a nominal Au concentration of 20 mM (116 nM nanoparticles). The grafting of GNRs with PEG helped achieve the adequate steric hindrance to prevent their flocculation in a variety of fluids, which would have severely disturbed their performances of photothermal and PA conversion.[7,15] The dimensions of the GNRs, measured using a transmission electron microscope, are 53 nm length and 11 nm axial diameter [Fig. 2(a)] with the longitudinal plasmon peak at 840 nm.[7]

2.4 Photoacoustic Measurements

Photoacoustic measurements were performed with a commercial PA imaging system from VisualSonics Inc. (Vevo LAZR, VisualSonics Inc., Toronto) that produces PA images coregistered with B-mode images of the surrounding structures. A full description of the system design is available in Ref. 28. PA signals were excited by a pulsed (20 Hz, 6 to 8 ns pulse width) and tunable (680 to 970 nm) Nd:YAG laser with an optical parametric oscillator to illuminate the sample through two rectangular fiber-optic bundles placed on both sides of a linear array transducer (13 to 24 MHz, 23 mm × 30 mm field of view) at an angle of 30 deg with the imaging plane. The acquisition time for the absorption spectrum acquisitions was ~60 s for 146 wavelengths (2 nm step).

The PA response from P1 and P2, which were filled by water, was tested. A 0.5 cm agar layer was deposited on the PDMS microfluidic device during PA measurements as a coupling material to at least maintain the six channels at a 1 cm depth (laser focus depth).

P1 was filled with ICG solution 1 mM and the absorption spectrum was acquired. The dynamic variation of the PA signal during 11 min was studied.

P1 was filled with PEG-GNRs at a dilution of 87 nM (15 mM Au dilution). P2 was filled with PEG-GNRs of three different dilutions: 87, 58, and 12 nM (15, 10, and 1 mM Au dilutions). The absorption spectrum of the nanoparticles was acquired with P1 and P2 and then compared to that acquired with a Jasco V-560 spectrophotometer [Fig. 2(b)].

The PA signal linearity with the number of nanoparticles in the sample was verified in two ways: through a linear fit of the signal amplitude for three different PEG-GNR dilutions in P2 and through a linear fit of the signal amplitude for the channels of different sections filled with the same nanoparticle dilution in P1.

The dynamic variation of the PA signal during 8 min was studied. The signal-to-noise ratio (SNR) and the contrast (C) were employed as image quality parameters and estimated according to the following equations:

$$\text{SNR} = \frac{s - b}{\sqrt{n_b^2 + n_s^2}}, \tag{1}$$
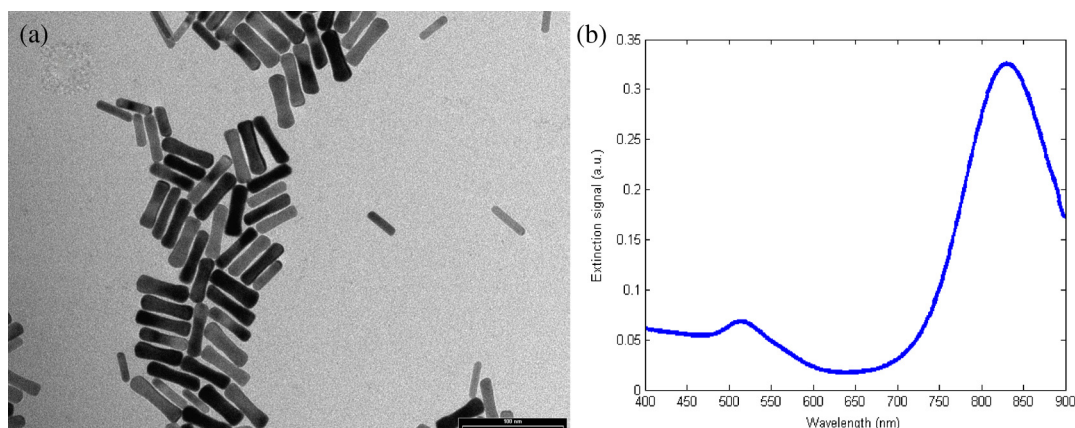
Fig. 2 Polyethylene glycol gold nanorods (PEG-GNRs): (a) TEM image and (b) absorption spectrum acquired with the spectrophotometer.
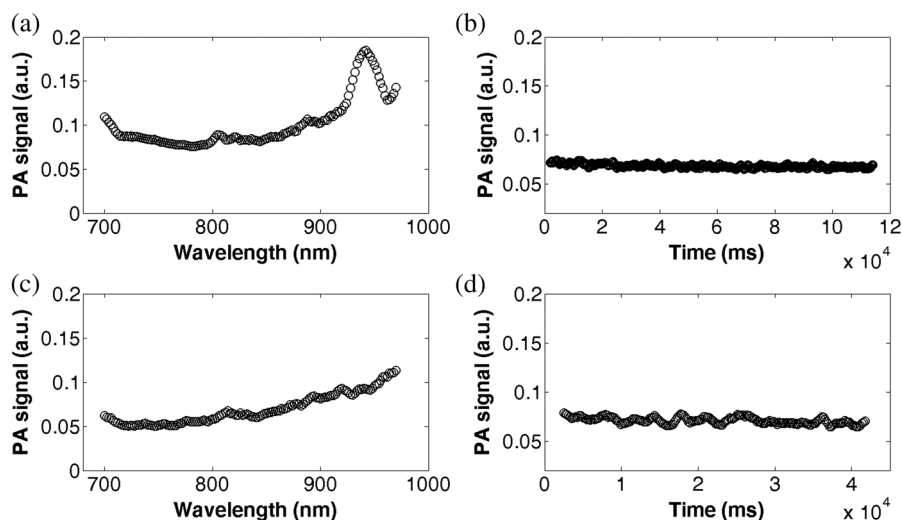
Fig. 3 Absorption spectrum and photoacoustic (PA) signal during time of [(a) and (b)] P2 and [(c) and (d)] P1 filled by water.

$$C = \frac{s - b}{b}, \tag{2}$$

where s (b) and n_s (n_b) are the average signal and its standard deviation in the region of interest on the GNR sample (background), respectively.

PA tests were performed in order to compare the signal generated by the TM-PDMS and the biological tissue (a region of mouse spleen at 2 mm of depth under the skin was considered).

3 Results

Neither P1 nor P2 showed a measurable PA response to the laser irradiation when filled with water. As shown in Fig. 3, the signal intensity was stable and comparable to the background.

Figure 4 shows a superimposition of the B-mode image (gray levels) and the PA signal intensity (red) of P1 loaded with ICG where all six channels are clearly distinguishable. Figure 5 shows the ICG absorption spectrum acquired for each micrometric channel of P1, which is characterized by an absorption peak between 800 and 900 nm. The dynamic variation of the PA signal of ICG loaded into P1 and irradiated for 11 min was tested and reported in Fig. 6. After 11 min, the signal was decreased with respect to the initial signal by 14% in the 500 μm channel, 17% in the 400 μm channel, 13% in the 300 μm channel, 9% in the 200 μm channel, 14% in the 100 μm channel, and 11% in the 50 μm channel.

Figures 7(a) and 7(b) show a superimposition of the B-mode image (gray levels) and the PA signal intensity (red) produced by GNRs loaded in P1 and P2, respectively. The absorption spectra of PEG-GNRs measured in both phantoms were in agreement with that measured with the spectrophotometer, with a resonance peak at ~840 nm [Figs. 8(a) and 8(b)]. The GNR concentration is fixed in all the channels of P1 (87 nM), while the volume acquired for each channel varies according to its geometrical constraints: the PA signal intensity is thus directly proportional to the number of GNRs. The number of excited nanorods can be estimated using the following equation:

$$N = CV, \tag{3}$$

where C is the nanoparticle dilution (nM) and V is the volume of interest (mm^3). To calculate V, the section A of the channel and the thickness z of the region of interest are needed. Because the thickness z is the same for all acquisitions, it can be considered as a constant. Then, Eq. (3) becomes
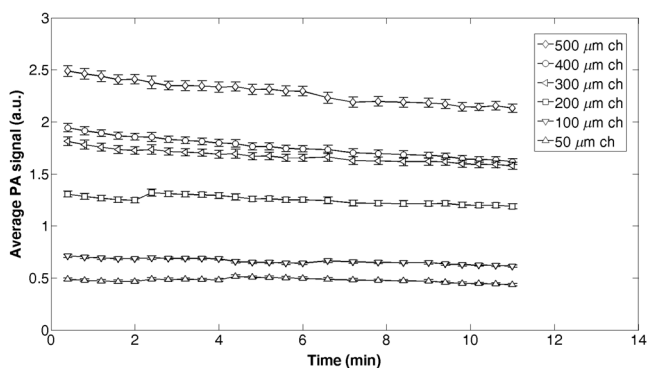
$$n = CA, \tag{4}$$

which gives the number of nanoparticles per 1 mm of thickness. In the case of the channel with $A = 100 \times 50 \ \mu$m^2,
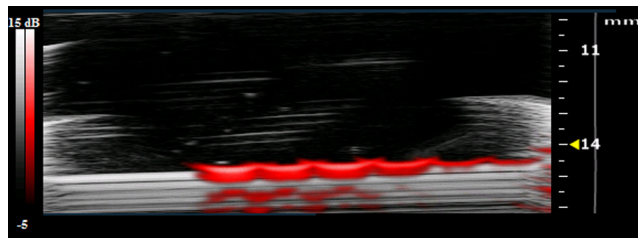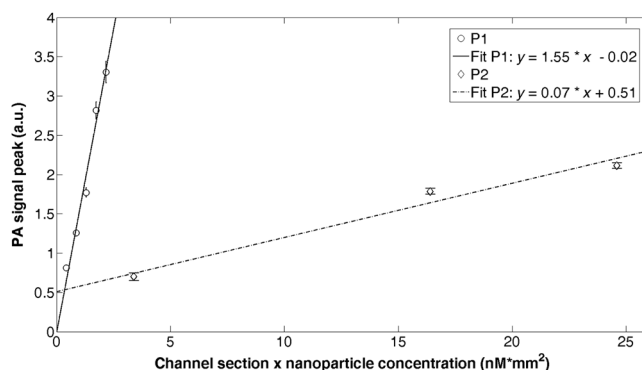

Fig. 4 PA images of P1 loaded with indocyanine green (ICG) solution 1 mM. B-mode image (gray levels) and PA signal (red) are superimposed.
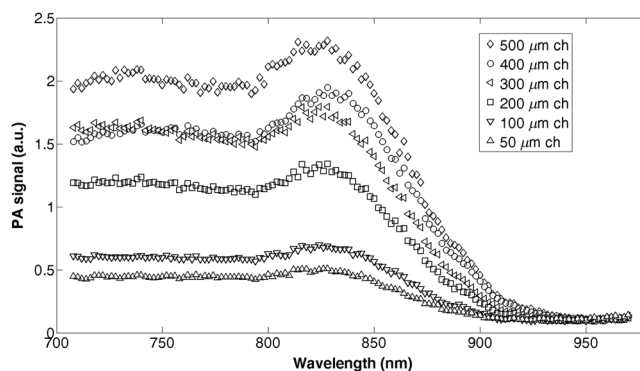

Fig. 5 Absorption spectrum of ICG solution 1 mM loaded into P1; each curve is relative to a channel (ch).

Fig. 6 PA average signal acquired with P1 loaded with ICG solution 1 mM, irradiated for 11 min; each curve is relative to a channel (ch).

Fig. 9 Peak signal versus nanoparticle concentration multiplied by the channel section for P1 loaded with PEG-GNRs 87 nM (circles and continuous line) and for P2 loaded with PEG-GNRs at three different dilutions (87, 58, and 12 nM) (rhombus and dotted line).
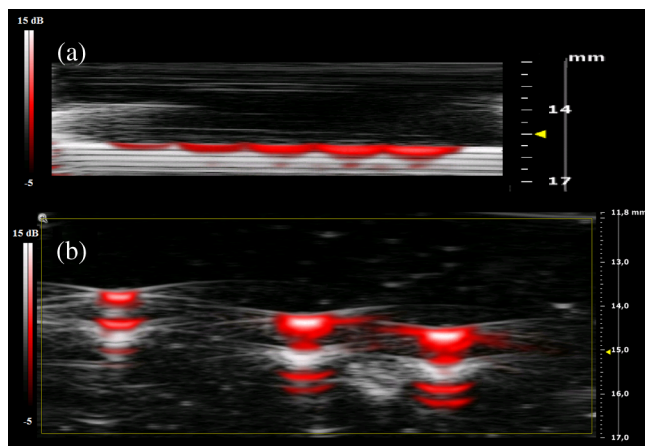
Fig. 7 (a) PA images of P1 loaded with PEG-GNRs 87 nM and (b) P2 loaded with PEG-GNRs at three different dilutions: 87, 58, and 12 nM. B-mode image (gray levels) and PA signal (red) are superimposed.

$n = 0.44 \ \text{nM} \cdot \text{mm}^2$, therefore the estimated limit to the detectable nanoparticle number is $< 0.44 \ \text{nM} \cdot \text{mm}^2$.

Figure 9 shows the PA signal peak as a function of the number of acquired nanoparticles (the x axis shows the nanoparticle concentration multiplied by the channel area in $\text{nM} \cdot \text{mm}^2$). The

slope of the curve for P1 ($1.55 \ \text{nM}^{-1} \cdot \text{mm}^{-2}$) is one order of magnitude higher than for P2 ($0.07 \ \text{nM}^{-1} \cdot \text{mm}^{-2}$).

The dynamic variation of the PA signal of PEG-GNRs during 8 min was tested. A decrease in the PA signal was measured in both types of phantoms [Figs. 10(a) and 10(b)]. In P1, after 8 min, the signal was decreased with respect to the initial signal by 20% in the 500 μm channel, 26% in the 400 μm channel, 13% in the 300 μm channel, 15% in the 200 μm channel, and 21% in the 100 μm channel. In P2, the signal was decreased with respect to the initial signal by 11% in the 87 nM tube, and 12% in the 58 nM tube; the signal did not show a decreasing trend in the 12 nM tube.

SNR and contrast produced by PEG-GNRs loaded into P1 and P2 were estimated as shown in Fig. 11. The results showed that the contrast and SNR produced by the same number of nanoparticles were higher (up to 50% for SNR and up to 300% for contrast) in P1 than in P2.

In Fig. 12, the absorption spectrum of the TM-PDMS, the PDMS, and the mouse spleen are shown. The TM-PDMS generates a twofold higher PA signal with respect to the PDMS. The mouse tissue absorption spectrum is characterized by an increasing absorption from 700 to 900 nm. The PA signal generated by the TM-PDMS, unlike PDMS, is comparable to that of biological tissue.
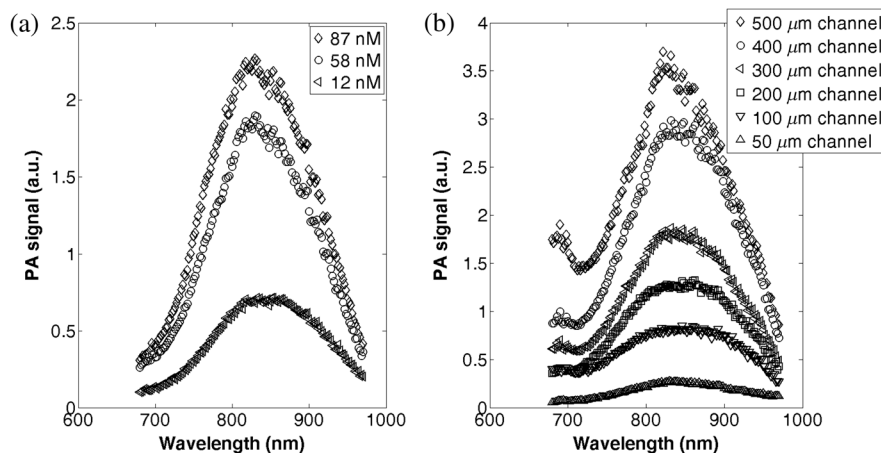

Fig. 8 (a) Absorption spectrum of PEG-GNRs at three different dilutions (87, 58, and 12 nM) in P2 and (b) PEG-GNRs 87 nM in P1; each curve is relative to a channel.
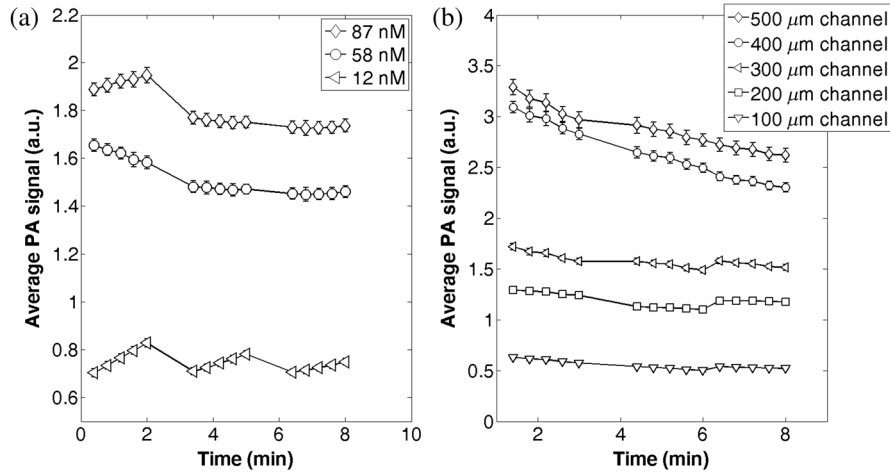
Fig. 10 PA average signal of PEG-GNRs, acquired during 8 min, loaded (a) in P2 (87 nM rhombus, 58 nM circles, 12 nM triangles) and (b) in P1 (500 μm channel rhombus, 400 μm channel circles, 300 μm channel left-pointing triangles, 200 μm channel squares, 100 μm channel upward-pointing triangles), loaded with PEG-GNRs, irradiated for 8 min.
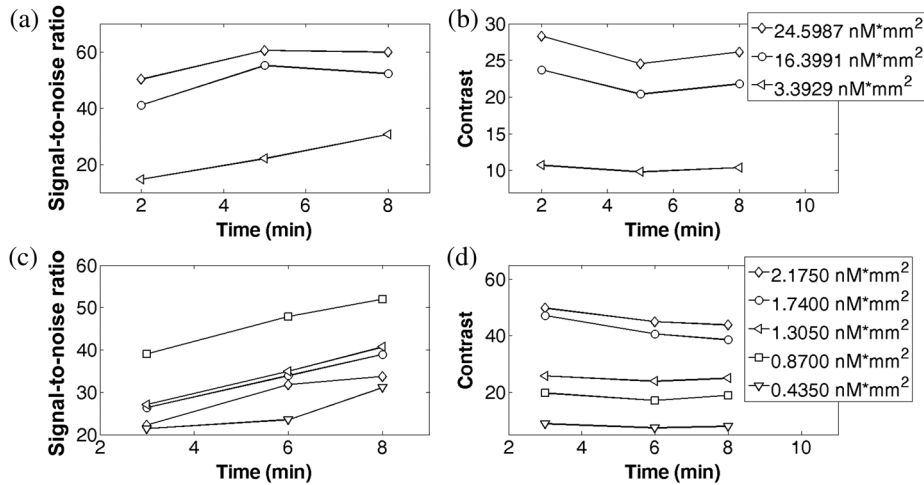
Fig. 11 P2 loaded with PEG-GNRs at three different dilutions [87 nM (24.6 nM $*$ mm^2) rhombus, 58 nM (16.4 nM $*$ mm^2) circles, 12 nM (3.4 nM $*$ mm^2) triangles] irradiated for 8 min: (a) signal-to-noise ratio and (b) contrast trends over time. P1 loaded with PEG-GNRs 87 nM [500 μm channel (2.2 nM $*$ mm^2) rhombus, 400 μm channel (1.7 nM $*$ mm^2) circles, 300 μm channel (1.3 nM $*$ mm^2) left-pointing triangles, 200 μm channel (0.87 nM $*$ mm^2) squares, 100 μm channel (0.44 nM $*$ mm^2) upward-pointing triangles] irradiated for 8 min: (c) signal-to-noise ratio and (d) contrast trends over time.
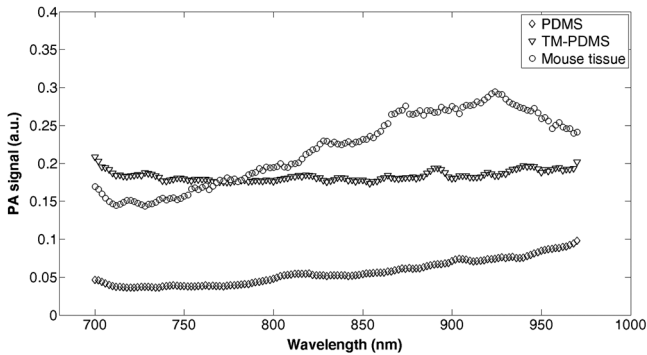
Fig. 12 Absorption spectrum of PDMS (rhombus), TM-PDMS (down-pointing triangles), and mouse tissue (region of mouse spleen at 2 mm of depth under the skin) (circles).

4 Conclusions

A microstructure PDMS device was designed, prepared and tested using PA experiments loaded with standard ICG dye and compared to an agar phantom through PEG-GNRs.

PDMS phantom is particularly promising in the field of photoacoustics. It is stable for months, durable against rough handling, and non-toxic during preparation and application.[16] It could be cleaned and reused, and the preparation time is fast. Furthermore, it did not show a signal response to the laser irradiation when filled with water. PDMS allowed reaching a lower detection limit compared to the agar phantom. This might be due to the higher acoustic attenuation of the polyethylene tubes, which causes a significant loss of the emitted PA signal. Therefore, the use of PDMS is preferable for the evaluation of the signal enhancement produced by different materials as

compared to agar. Moreover, this phantom, with its exceptionally fine geometry (of the order of tens of micrometers), enables the estimation of a range for the minimum detectable nanoparticle number. A decrease in the PA signal generated by PEG-GNRs was observed over time; we hypothesize that it was due to phenomena such as nanoparticle reshaping.[29] If this hypothesis is correct, the development of phantoms would be essential for the study of these processes, which is crucial to achieve a deeper understanding of the behavior of a contrast agent under different conditions.

By adding titanium dioxide and black ink to the PDMS, the absorption and reduced scattering coefficients were tuned in order to be similar to those of biological tissues. Our results confirm that the TM-PDMS mimics the tissue properties within the scope of PA imaging, and this kind of phantom can be employed as a model of soft tissue.

Future tests will be conducted by using our original PDMS phantom for investigating the spatial resolution of the PA system as a function of the contrast agent dilution. Furthermore, future experiments will be performed by using this phantom as a device that enables the estimation of the minimum number of nanoparticles that can be injected *in vivo* to obtain a detectable PA signal.

Acknowledgments

References

1. P. Beard, "Biomedical photoacoustic imaging," *Interface Focus* **1**(4), 602–631 (2011).
2. L. V. Wang, "Multiscale photoacoustic microscopy and computed tomography," *Nat. Photon.* **3**(9), 503–509 (2009).
3. X. Yang et al., "Nanoparticles for photoacoustic imaging," *Wiley Interdiscip. Rev. Nanomed. Nanobiotechnol.* **1**(4), 360–368 (2009).
4. M. A. Hahn et al., "Nanoparticles as contrast agents for *in-vivo* bioimaging: current status and future perspectives," *Anal. Bioanal. Chem.* **399**(1), 3–27 (2011).
5. S. Manohar, C. Ungureau, and T. G. Van Leewen, "Gold nanorods as molecular contrast agents in photoacoustic imaging: the promises and the caveats," *Contrast Media Mol. Imaging* **6**, 389–400 (2011).
6. X. Huang et al., "Gold nanoparticles: interesting optical properties and recent applications in cancer diagnostics and therapy," *Nanomed. (Lond)* **2**, 681–693 (2007).
7. F. Ratto et al., "Gold nanorods as new nanochromophores for photothermal therapies," *J. Biophotonics* **4**, 64–73 (2011).
8. M. Eghtedari et al., "High sensitivity of *in vivo* detection of gold nanorods using a laser optoacoustic imaging system," *Nano Lett.* **7**, 1914 (2007).
9. K. Kim et al., "Photoacoustic imaging of early inflammatory response using gold nanorods," *Appl. Phys. Lett.* **90**, 223901 (2007).
10. P.-C. Li et al., "Photoacoustic imaging of multiple targets using gold nanorods," *IEEE Trans. Ultrason. Ferroelectr. Freq. Control* **54**, 1642 (2007).
11. A. Agarwal et al., "Targeted gold nanorod contrast agent for prostate cancer detection by photoacoustic imaging," *J. Appl. Phys.* **102**, 064701 (2007).
12. K. Song et al., "Noninvasive *in vivo* spectroscopic nanorod-contrast photoacoustic mapping of sentinel lymph nodes," *Eur. J. Radiol.* **70**, 227 (2009).
13. A. Taruttis et al., "Real-time imaging of cardiovascular dynamics and circulating gold nanorods with multispectral optoacoustic tomography," *Opt. Express* **18**, 19592 (2010).
14. D. Pan et al., "A facile synthesis of novel self-assembled gold nanorods designed for near-infrared imaging," *J. Nanosci. Nanotechnol.* **10**(12), 8118–8123 (2010).
15. F. Ratto et al., "Size and shape control in the overgrowth of gold nanorods," *J. Nanopart. Res.* **12**, 2029–2036 (2010).
16. K. Zell et al., "Acoustical properties of selected tissue phantom materials for ultrasound imaging," *Phys. Med. Biol.* **52**, N475–N484 (2007).
17. J. Cook, R. Bouchard, and S. Emelianov, "Tissue-mimicking phantoms for photoacoustic and ultrasonic imaging," *Biomed. Opt. Express* **2**, 3193–3206 (2011).
18. S. E. Bohndiek et al., "Development and application of stable phantoms for the evaluation of photoacoustic imaging instruments," *PLoS One* **8**(9), e75533 (2013).
19. H. G. Akarçay et al., "Determining the optical properties of a gelatin-TiO_2 phantom at 780 nm," *Biomed. Opt. Express* **3**(3), 418–434 (2012).
20. C. Sun et al., "The speed of sound and attenuation of an IEC agar-based tissue-mimicking material for high frequency ultrasound applications," *Ultrasound Med. Biol.* **38**(7), 1262–1270 (2012).
21. J. Hammer et al., "A facile method to fabricate hydrogels with micro-channel-like porosity for tissue engineering," *Tissue Eng. Part C Methods* **20**(2), 169–176 (2014).
22. L. E. Bertassoni et al., "Hydrogel bioprinted microchannel networks for vascularization of tissue engineering constructs," *Lab Chip* **14**, 2202 (2014).
23. International Commission on Radiation Units, and Measurements, "Tissue substitutes, phantoms and computational modeling in medical ultrasound," ICRU REPORT 61 (1998).
24. F. Sabri et al., "*In vivo* ultrasonic detection of polyurea crosslinked silica aerogel implants," *PLoS One* **8**(6), e66348 (2013).
25. T. Buma et al., "High frequency ultrasonic imaging using optoacoustic arrays," in *Proc. of Ultrasonic Symp.*, Vol. 1, pp. 571–580, IEEE (2002).
26. F. Ayers et al., "Fabrication and characterization of silicone-based tissue phantoms with tunable optical properties in the visible and near infrared domain," *Proc. SPIE* **6870**, 687007 (2008).
27. R. Long et al., "Optofluidic phantom mimicking optical properties of porcine livers," *Biomed. Opt. Express* **2**(7), 1877–1892 (2011).
28. A. Needles et al., "Development of a combined photoacoustic micro-ultrasound system for estimating blood oxygenation," in *IEEE Ultrasonics Symp.*, pp. 390–393 (2010).
29. L. Cavigli et al., "Size affects the stability of the photoacoustic conversion of gold nanorods," *J. Phys. Chem. C* **118**(29), 16140–16146 (2014).

Cinzia Avigo is a research fellow at the Institute of Clinical Physiology of the National Research Council, Pisa, Italy. She received her BSc and MSc degrees in physics from the University of Pisa. She is now enrolled in the second year of the Specialty School on Medical Physics and her current research interest include the *in vitro* and *in vivo* characterization of novel contrast agents for photoacoustic imaging.

Nicole Di Lascio learned her master's degree in biomedical engineering from the University of Pisa in 2011. She has worked at the Institute of Clinical Physiology of the National Research Council in the field of innovative cardiovascular biomarkers from signal and image processing. She is currently a PhD student in translational medicine at the Institute of Life Science of Scuola Superiore Sant'Anna. Her research interests and activities are mainly focused on ultrasound and photoacoustic imaging.

Francesco Faita has been working as a research fellow at the Institute of Clinical Physiology since 2001. His main research interests lie in biomedical imaging, in particular in the field of ultrasound and photoacoustic. A major focus of his research is the development of methodologies for cardiovascular analysis in clinical and animal models. He is the author of 58 scientific publications in international journals and conference proceedings.

Luca Menichetti developed his interests in the field of tracer chemistry for medical applications, moving from radiochemistry to other imaging modalities, such as magnetic resonance spectroscopy exploiting the hyperpolarization of 13C-molecules and the development of novel multimodality based on nanostructured multifunctional materials and photoacoustic imaging. He is a contract professor at the Department of Chemistry at the University of Pisa and is the scientific coordinator of national projects in the field of nanomedicine.

Biographies for the other authors are not available.